Ultrafast Spectroscopy of Midinfrared Internal Exciton Transitions in Separated Single-Walled Carbon Nanotubes

Jigang Wang,[1,2] Matt W. Graham,[3] Yingzhong Ma,[3,4] Graham R. Fleming,[3] and Robert A. Kaindl[1]

[1]*Materials Sciences Division, E. O. Lawrence Berkeley National Laboratory, Berkeley, California 94720, USA*
[2]*Department of Physics and Astronomy and Ames Laboratory, Iowa State University, Ames, Iowa 50010, USA*
[3]*Department of Chemistry, University of California at Berkeley and Physical Biosciences Division, E. O. Lawrence Berkeley National Laboratory, Berkeley, California 94720, USA*
[4]*Chemical Sciences Division, Oak Ridge National Laboratory, Oak Ridge, Tennessee 37831, USA*

(Received 2 November 2009; published 26 April 2010)

We report a femtosecond midinfrared study of the broadband low-energy response of individually separated (6,5) and (7,5) single-walled carbon nanotubes. Strong photoinduced absorption is observed around 200 meV, whose transition energy, oscillator strength, resonant chirality enhancement, and dynamics manifest the observation of quasi-one-dimensional intraexcitonic transitions. A model of the nanotube $1s$-$2p$ cross section agrees well with the signal amplitudes. Our study further reveals saturation of the photoinduced absorption with increasing phase-space filling of the correlated e-h pairs.

DOI: 10.1103/PhysRevLett.104.177401 PACS numbers: 78.67.Ch, 78.30.Na, 78.47.J−

The quasi-one-dimensional (quasi-1D) confinement of photoexcited charges in single-walled carbon nanotubes (SWNTs) gives rise to strongly enhanced Coulomb interactions and large exciton binding energies on the 100 meV energy scale. These amplified electron-hole (e-h) correlations are a key aspect of nanotube physics [1]. With the availability of individually separated SWNT ensembles, this strong excitonic behavior was confirmed by interband absorption-luminescence maps [2], two-photon excited luminescence [3,4], and ultrafast spectroscopy [5]. Optical interband probes, however, are limited by symmetry and momentum to detect only a small subset of excitons.

As illustrated in Fig. 1(a), in a two-particle scheme, SWNT excitons are characterized by a center-of-mass momentum K and by an internal quantum state (designated here as $1s$, $2s$, $2p$, ...) that accounts for the relative charge motion. Each state splits into even (g) and odd (u) parity levels corresponding to different superpositions of the cell-periodic wave functions of the underlying graphene lattice [4]. This entails a series of optically "dark" excitons, including the $1s$-(g) lowest-energy exciton that lacks coupling in both single- and two-photon interband spectroscopy [3,4]. Splitting into singlet and triplet spin states additionally restricts interband optical coupling [6]. Finally, interband transitions are limited to excitons around $K \approx 0$ due to momentum conservation.

Intraexcitonic transitions between low-energy levels of excitons with the same cell-periodic symmetry [arrows, Fig. 1(a)] represent a fundamentally different tool, analogous to atomic absorption spectroscopy. In contrast to interband absorption that measures the ability to *generate* e-h pairs, intraexcitonic absorption detects existing excitons via transitions from the $1s$ ground state to higher relative-momentum states [7,8]. Being independent of K, it is sensitive to genuine exciton populations across momentum space. As the cell-periodic component of the wave function remains unchanged, intraexcitonic absorption is also unrestricted by the exciton ground state symmetry [7]. Applied to individualized SWNTs, intraexcitonic resonances can thus measure both bright and dark excitons and should occur in the midinfrared (mid-IR) after ultrafast excitation. In contrast to extensive interband nanotube studies [9–12], only a few ultrafast intraband experiments have been carried out which focus largely on nanotube bundles [13–16]. THz experiments on photoexcited bundled tubes revealed a non-Drude response attributed to small-gap metallic tubes or intertube charge separation [13,14]. Mid-IR transient absorption was also observed in bundled nanotubes and assigned to transitions from allowed to dipole-forbidden excitons [15,16].

In this Letter, we report ultrafast optical-pump, mid-IR-probe studies of individually separated (6,5) and (7,5) SWNTs. Transient spectra after photoexcitation evidence strong mid-IR absorption around 200 meV, in accordance with intraexcitonic transitions of strongly bound e-h pairs in semiconducting nanotubes. The absorption cross section

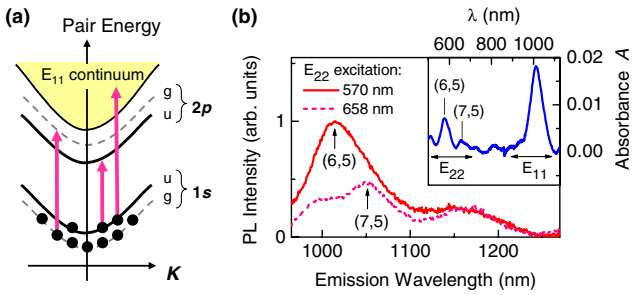

FIG. 1 (color online). (a) Two-particle e-h *pair* dispersion, illustrating exciton bands and $1s \rightarrow 2p$ intraexcitonic transitions (arrows). (b) Photoluminescence (PL) spectra of the sample under resonant E_{22} excitation. Inset: Near-IR absorbance after subtracting background scattering.

of 4×10^{-15} cm^2 agrees closely with calculations of quasi-1D intraexcitonic $1s$-$2p$ dipole transitions presented here. The excitation-wavelength dependence and kinetics further underscore the excitonic origin of the mid-IR response, and its intensity dependence scales quantitatively with a model of phase-space filling expected for quasi-1D excitons. This intraexcitonic absorption represents a sensitive tool to probe correlated e-h pairs in SWNTs, unhindered by interband dipole or momentum restrictions.

Ultrafast spectroscopy was carried out in transmission using widely tunable femtosecond (fs) pulses in the mid-IR and visible range. Two near-IR optical parametric amplifiers (OPAs) were pumped by a 1 kHz, 28 fs Ti:sapphire amplifier. Resonant and off-resonant interband excitation was achieved using the frequency-doubled OPA or a fraction of the fundamental. The output of the second OPA was difference-frequency mixed in GaSe to generate ≈100 fs mid-IR probe pulses tunable from 4 to 12 μm [17]. We study individually separated Co-Mo-catalyst-grown SWNTs of mainly (6,5) and (7,5) chiralities [18] embedded in 50-μm-thick polyethylene (PE). Importantly, PE ensures transparency throughout our mid-IR probe range, except for a narrow CH-bend vibration at 178 meV. The films were fabricated by drying PE solutions in decalin mixed with micelle-dispersed SWNTs, after transferring SWNTs suspended with NaDDBS in H_2O to the PE solution via ultrasound and thermal treatments. In Fig. 1(b), the sample's photoluminescence (PL) spectra for resonant (6,5) and (7,5) E_{22} excitation clearly exhibit the distinct E_{11} emission of these individualized SWNT chiralities, with only weak emission from bundled tubes around 1160 nm [19]. The absorption spectrum [inset, Fig. 1(b)] also exhibits the distinct E_{11} and E_{22} absorption peaks.

Ultrafast spectrally resolved mid-IR transmission changes $\Delta T/T$ are shown in Fig. 2 for different time delays Δt after 800 nm photoexcitation at room temperature. A strong photoinduced absorption appears within the time resolution after photoexcitation [Fig. 2(b), $\Delta t = 200$ fs] and decays on a ps time scale [Figs. 2(c) and 2(d)]. The transient spectra are characterized by a broadly sloping, asymmetric resonance around 200 meV, with a rapid onset above 160 meV. This mid-IR resonance occurs in the transparent region far below the lowest interband exciton ($E_{11} \simeq 1.2$ eV) and intersubband transitions ($E_{22} - E_{11} \geq 0.6$ eV). The peak energy is close to the (6,5) and (7,5) $1s$-$2p$ energy splitting in two-photon luminescence studies and calculations [3,4,20]. Thus, we associate this absorption with intraexcitonic transitions between $1s$ and $2p$ exciton levels of opposite parity. Both dipole-allowed and optically dark $1s$ excitons can fundamentally contribute to this response. The dynamics exhibits a pulse-width limited rise of the photoinduced mid-IR absorption (inset, Fig. 2), which indicates rapid exciton formation.

We should comment on the asymmetric line shape observed in Fig. 2. The observed rapid onset and asymmetry point to a predominantly inhomogeneous broadening, resulting in a large ≃100 meV line width composed of multiple transitions, which matches well with similar spectral features in two-photon PL experiments [3,4]. We attribute the higher-energy tail to intraexcitonic transitions from the $1s$ into higher-lying np bound states and into the broad continuum of unbound pairs, consistent with the asymmetric intraexcitonic spectra of quasi-2D e-h pairs [8]. Note that a much narrower peak seems to exist around 170 meV, which we assign as an artifact [21]. Low-energy absorption is also observed below 160 meV which can arise, e.g., from fluctuations of the dielectric environment around the nanotube and other chiral tube species [22].

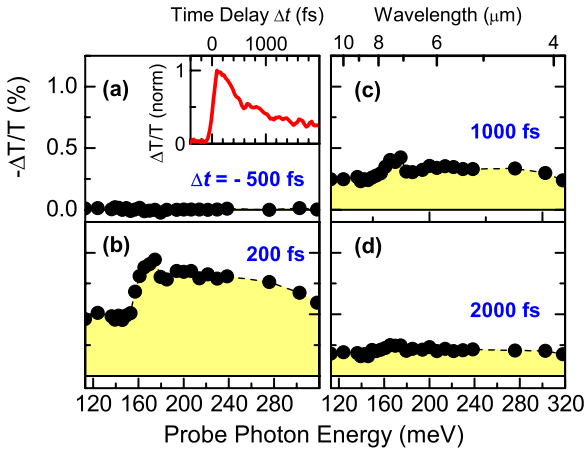

FIG. 2 (color online). (a)–(d) Ultrafast spectrally resolved mid-IR transmission changes after 800 nm excitation for four different delays Δt as indicated. Inset: normalized dynamics of the mid-IR transmission probed at 4.4 μm wavelength.

To further substantiate the nature of the response, Fig. 3(a) shows the excitation-wavelength dependence. Resonant photoexcitation of the (6,5) and (7,5) interband E_{22} transitions, at 572 nm and 697 nm, respectively, leads to significant enhancement of the transient mid-IR absorption. The amplitude closely tracks the PL-excitation spectrum [Fig. 3(b)], which clearly underscores the tube-specific origin of the transient mid-IR response. This conclusion is further supported by the disappearance of the photoinduced signal for excitation below the E_{11} transition [1250 nm, Fig. 3(a)]. Hence, the observed photoinduced absorption arises from intraexcitonic transitions of (6,5) and (7,5) SWNTs. The mid-IR dynamics after (6,5) E_{22} excitation is shown in Fig. 3(c) on an extended time scale, revealing a strongly nonexponential decay [dots, Fig. 3(c)] over several 10 ps. The dynamics closely follows the E_{11} exciton bleaching [solid line, Fig. 3(c)], confirming that the mid-IR signals originate from excitations in the E_{11} manifold. Thermal broadening $k_BT \simeq 26$ meV at 300 K entails comparable occupation of dark and bright excitons (split by ≃10 meV), which enables this comparison. The decay has a bimolecular shape [dashed line, Fig. 3(c)], similar to the fs kinetics of excitons in individualized SWNT suspensions explained by exciton-exciton annihilation [9], which further underscores the excitonic origin of the mid-IR response.

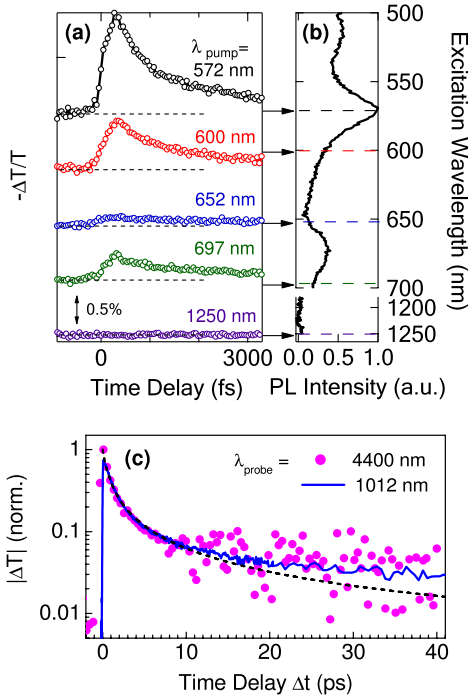

FIG. 3 (color online). (a) Pump wavelength dependence resonant and off-resonant to the (6,5) and (7,5) E_{22} transitions. Traces are offset for clarity, and measured at 4.4 μm with 260 μJ/cm^2 excitation fluence. (b) PL-excitation spectrum for fixed E_{11} emission at 1012 nm. (c) Normalized mid-IR dynamics (dots) after 572 nm excitation. Thick line: E_{11} transmission change, scaled to the mid-IR signal at long delays. Dashed line: bimolecular decay $|\Delta T| \propto (1+\gamma t)^{-1}$ with $\gamma = 1.5$ ps^{-1}.

The mid-IR transmission changes can be used to estimate the absorption cross section $\sigma^{\parallel}_{\mathrm{MIR}}$ of the intraexcitonic transition, whose dipole is oriented parallel to the SWNT axis. It is defined as $\sigma^{\parallel}_{\mathrm{MIR}} = 3\ln(1-\Delta T/T)/n_{\mathrm{exc}}$, where ΔT is the initial transmission change and n_{exc} the photoexcited density. The factor 3 accounts for the random SWNT orientation. Considering (6,5) E_{22} resonant excitation in Fig. 3(a), one has $\Delta T/T \approx 1.7\%$ and $n_{\mathrm{exc}} = (F/\hbar\omega) \times \ln(10) A = 1.2 \times 10^{13}$ cm^{-2}, given $F = 260$ μJ/cm^2 and $A \simeq 0.007$ [inset, Fig. 1(b)]. This yields the experimentally derived value for the cross section of $\sigma^{\parallel}_{\mathrm{MIR}} \simeq 4 \times 10^{-15}$ cm^2.

For comparison, we calculate the intraexcitonic $1s$-$2p$ cross section based on a model of Wannier-like excitons in SWNTs. The normalized $1s$ and $2p$ wave functions of Coulomb-bound e-h pairs on a cylindrical surface are [23]

$$\psi_{1s}(x) = \sqrt{\frac{8}{(a_B^*)^3 \alpha_{1s}^3 B_{1s}}}\,|x|\, e^{-(|x|/a_B^* \alpha_{1s})}\, U\!\left(1-\alpha_{1s}, 2, \frac{2|x|}{a_B^* \alpha_{1s}}\right),$$
$$\psi_{2p}(x) = \sqrt{\frac{2}{(a_B^*)^3}}\, x\, e^{-(|x|/a_B^*)}, \qquad (1)$$

where x measures the distance along the nanotube axis and $a_B^* = 4\pi\epsilon\epsilon_0\hbar^2/\mu e^2$ is the effective 3D Bohr radius with reduced mass μ and permittivity ϵ. Furthermore, U is Kummer's confluent hypergeometric function of the second kind and $B_{1s} \equiv 2\int_0^\infty y^2 e^{-y}[U(1-\alpha_{1s}, 2, y)]^2 dy$ is a normalization constant. The binding energies are $E_{1s} = -\mathrm{Ry}^*/(\alpha_{1s})^2$ and $E_{2p} = -\mathrm{Ry}^*$, where $\mathrm{Ry}^* \equiv \hbar^2/(2\mu a_B^{*2})$ is the 3D effective Rydberg energy. Also, α_{1s} is a scaling parameter that depends on the SWNT nanotube radius r_{NT} via $\ln(\alpha_{1s}) - \Psi(1-\alpha_{1s}) - (2\alpha_{1s})^{-1} \equiv \ln(r_{\mathrm{NT}}) - 2\Psi(1)$ where Ψ is the digamma function [23]. For the (6,5) and (7,5) SWNTs studied here, we have $r_{\mathrm{NT}} \simeq 0.4$ nm which entails $\alpha_{1s} = 0.33$, and $\mu \simeq 0.067$ from interpolated carrier effective masses [24]. The scale and shape of the resulting exciton wave functions are shown in Fig. 4(a). For this, the permittivity which depends on the local dielectric environment was adjusted to $\epsilon = 6$ to reproduce the intraexcitonic splitting $E_{2p} - E_{1s} \simeq 0.2$ eV from the experiment, which corresponds to a binding energy of 233 meV.

With the above, we obtain the $1s$-$2p$ intraexcitonic oscillator strength of quasi-1D excitons in SWNTs:

$$f_{1s\to 2p} \equiv \frac{128\mu a_B^2 \alpha_{1s}^5}{\hbar^2 B_{1s}}(E_{2p} - E_{1s}) \times \left(\int_0^\infty s^3 e^{-s(1+\alpha_{1s})} U(1-\alpha_{1s}, 2, 2s) ds\right)^2. \qquad (2)$$

For our specific parameters, $f_{1s\to 2p} = 0.41$. Transitions into higher bound np levels ($n > 2$) were also calculated but are very weak and add less than 15% in spectral weight. The *spectrally integrated* absorption cross section is then determined as $\sigma^{\mathrm{Int}}_{1s\to 2p} = 2\pi^2 e^2/(4\pi\epsilon_0 \mu c n) \times f_{1s\to 2p} = 4.4 \times 10^{-13}$ cm^2 meV, where $n = 1.5$ is the polymer refractive index. Spreading this absorption across $\approx$100 meV results in an estimated $1s$-$2p$ intraexcitonic cross section of $\sigma_{1s\to 2p} \simeq 4.4 \times 10^{-15}$ cm^2, in very close agreement with our experiment. Full modeling of the asymmetric mid-IR intraexcitonic line shape in Fig. 2 is beyond the scope of the Wannier-exciton model. However, the above illustrates a general consistency between the observed mid-IR signal amplitude and the quasi-1D $1s$-$2p$ intraexcitonic cross section, motivating more sophisticated theory to calculate bound-bound and bound-continuum spectra with chirality-specific SWNT wave functions.

The transient mid-IR absorption represents a strong oscillator comparable to the interband absorption. In the photoexcited state, this low-energy oscillator strength is derived via transfer from the interband exciton peaks, i.e., from E_{11} bleaching [10,11]. As plotted in Fig. 4(b), with increasing excitation fluence, the mid-IR amplitude $|\Delta T/T|$ exhibits a distinctly nonlinear behavior. This finding is well described by a saturation model $\Delta T \propto 1 - e^{-F/F_S}$, shown as the solid line in Fig. 4(b) for $F_S = 170$ μJ/cm^2. This corresponds to a 1D saturation density $n_s = \sigma_{22}^{\mathrm{eff}} \times F_s/\hbar\omega$, where $\sigma_{22}^{\mathrm{eff}}$ is the effective E_{22} absorption cross section per unit nanotube length. The cross section of (6,5) SWNTs was recently found to be $\sigma^{\parallel}_{22} \simeq 85$ nm$^2/\mu$m for light polarized parallel to the nanotube

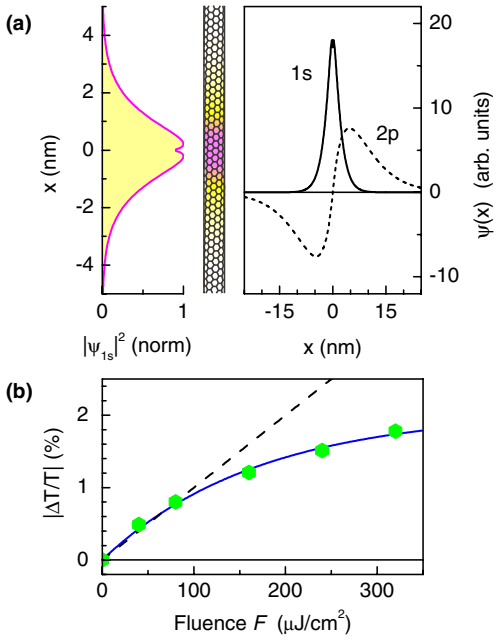

FIG. 4 (color online). (a) Squared wave function amplitude $|\psi_{1s}(x)|^2$ compared to the (6,5) SWNT scale (left), and bare $1s$ and $2p$ wave functions (right). (b) Pump fluence dependence of the initial mid-IR transmission change (dots) after resonant (6,5) E_{22} excitation. Solid line: model explained in the text. Dashed line: linear scaling (guide to the eyes).

axis, such that $\sigma_{22}^{\text{eff}} = 1/3 \times \sigma_{22}^{\parallel}$ [25]. This yields from our experiment a saturation density $n_S = 1.4 \times 10^6$ cm^{-1} corresponding to an average exciton spacing $d_{XX} \approx 7$ nm. The value is close to the saturation density extrapolated from E_{11} interband bleaching at lower densities [11], while surpassing the saturation of time-averaged PL by more than an order of magnitude [12]. The difference occurs since PL depends on density-dependent decay times that saturate at lower densities, while our study detects the initial pair density. For comparison, we consider phase-space filling (PSF), i.e., the increasing occupation of the constituent fermion states of the exciton many-particle wave function [26]. The PSF density is given by $N_S^{\text{PSF}} = L/[\sum_k \psi_k |\psi_k|^2 / \psi(x=0)]$, where ψ_k are the Fourier coefficients of the exciton wave function $\psi(x)$, and L is the normalization length [11,26,27]. For our quasi-1D $1s$ exciton wave function [Fig. 4(a)] this yields $N_S^{\text{PSF}} = 2.5 \times 10^6$ cm^{-1}. Hence, the mid-IR response approaches yet remains somewhat below the limit imposed by phase-space filling.

In conclusion, intraexcitonic transitions are both a direct consequence and a measure of e-h correlations. Our experiments provide new insights into the chirality-specific femtosecond mid-IR response of electronic excitations in individually separated SWNTs. A photoinduced absorption around 200 meV was observed, manifesting quasi-1D intraexcitonic transitions in close agreement with the calculated $1s$-$2p$ oscillator strength. The (6,5)/(7,5) chirality-specific enhancement and nonexponential kinetics of the transient mid-IR absorption further underscore its excitonic origin. We believe that the mid-IR probe, extended, e.g., into the low-temperature or low-density limit, will provide a versatile spectroscopic tool to investigate bound quasi-1D e-h pairs and their internal electronic structure independent of interband symmetry.

This work was supported by the Office of Science, U.S. DOE, via Contract No. DE-AC02-05CH11231 with initial provision from LDRD. Manuscript finalization was also supported by Ames Laboratory, DOE Contract No. DE-AC02-07CH11358. SWNTs were characterized at the Molecular Foundry, and prepared at U.C. Berkeley as supported by the NSF.

[1] See, e.g., M. S. Dresselhaus, G. Dresselhaus, R. Saito, and A. Jorio, Annu. Rev. Phys. Chem. **58**, 719 (2007).
[2] M. J. O'Connell *et al.*, Science **297**, 593 (2002).
[3] F. Wang *et al.*, Science **308**, 838 (2005).
[4] J. Maultzsch *et al.*, Phys. Rev. B **72**, 241402(R) (2005).
[5] Y.-Z. Ma *et al.*, in *Carbon Nanotubes*, edited by A. Jorio, G. Dresselhaus, and M. S. Dresselhaus, Topics Appl. Physics Vol. 111 (Springer Verlag, Berlin, 2008), p. 321.
[6] J. Jiang *et al.*, Phys. Rev. B **75**, 035407 (2007); E. B. Barros *et al.*, Phys. Rev. B **73**, 241406 (2006).
[7] T. Ideguchi, K. Yoshioka, A. Mysyrowicz, and M. Kuwata-Gonokami, Phys. Rev. Lett. **100**, 233001 (2008).
[8] R. A. Kaindl *et al.*, Nature (London) **423**, 734 (2003); Phys. Rev. B **79**, 045320 (2009).
[9] Y.-Z. Ma *et al.*, J. Chem. Phys. **120**, 3368 (2004); Phys. Rev. Lett. **94**, 157402 (2005).
[10] F. Wang *et al.*, Phys. Rev. B **70**, 241403(R) (2004); G. N. Ostojic *et al.*, Phys. Rev. Lett. **94**, 097401 (2005); O. J. Korovyanko *et al.*, Phys. Rev. Lett. **92**, 017403 (2004).
[11] L. Luer *et al.*, Nature Phys. **5**, 54 (2009).
[12] Y. Murakami and J. Kono, Phys. Rev. Lett. **102**, 037401 (2009).
[13] L. Perfetti *et al.*, Phys. Rev. Lett. **96**, 027401 (2006); T. Kampfrath *et al.*, Phys. Rev. Lett. **101**, 267403 (2008).
[14] M. C. Beard, J. L. Blackburn, and M. J. Heben, Nano Lett. **8**, 4238 (2008).
[15] H. Zhao *et al.*, Phys. Rev. B **73**, 075403 (2006).
[16] L. Luer *et al.*, Phys. Rev. B **80**, 205411 (2009).
[17] The probe was spectrally resolved (10 nm resolution).
[18] S. M. Bachilo *et al.*, J. Am. Chem. Soc. **125**, 11 186 (2003).
[19] O. N. Torrens *et al.*, Nano Lett. **6**, 2864 (2006).
[20] Differences in this splitting can arise from the dissimilar embedding matrices, i.e., dielectric constants.
[21] It appears due to a downward step at exactly the 178 meV vibrational resonance in the PE matrix.
[22] A. Jorio *et al.*, Phys. Rev. B **72**, 075207 (2005).
[23] H. D. Cornean, T. G. Pedersen, and B. Ricaud, Contemp. Math. **447**, 45 (2007).
[24] A. Jorio *et al.*, Phys. Rev. B **71**, 075401 (2005).
[25] S. Berciaud, L. Cognet, and B. Lounis, Phys. Rev. Lett. **101**, 077402 (2008).
[26] S. Schmitt-Rink, D. S. Chemla, and D. A. B. Miller, Phys. Rev. B **32**, 6601 (1985).
[27] B. I. Greene *et al.*, Phys. Rev. Lett. **58**, 2750 (1987).